Surfaces and Interfaces 76 (2025) 107873

Contents lists available at ScienceDirect

Surfaces and Interfaces

journal homepage: www.sciencedirect.com/journal/surfaces-and-interfaces

Upcycled coffee waste-derived carbon nanoparticles@Ag nanostructures via microwave-assisted synthesis for efficient tetracycline photodegradation

S. Bettini [a,b], R. Pagano [a], M. Ottolini [a], L. Valli [a,b], G. Giancane [b,c,*]

[a] Department of Biological and Environmental Sciences and Technologies, University of Salento, Via per Monteroni, Lecce, 73100, Italy
[b] National Interuniversity Consortium of Materials Science and Technology (INSTM), Via G. Giusti, 9 50121 Firenze Italy
[c] Department of Cultural Heritage, University of Salento, Via D. Birago 64, Lecce, 73100, Italy

ARTICLE INFO

Keywords:
Sustainable materials
Photocatalysis
Carbon-based composites
Silver nanoparticles
Microwave synthesis
Antibiotic degradation

ABSTRACT

The increasing presence of tetracycline antibiotics in aquatic environments poses serious ecological and health risks due to their persistence and potential to promote antibiotic resistance. In this study, we report a sustainable and efficient strategy for the photocatalytic degradation of tetracycline using Ag-decorated carbon nanoparticles synthesized via a rapid microwave-assisted method. The carbonaceous component was derived from spent coffee grounds, promoting a circular economic approach. Structural, optical, and vibrational analyses (UV–Vis, FTIR, Raman, TERS, and XRD) reveal significant transformations in both the carbon matrix and silver phase, enabling enhanced photocatalytic activity. The optimized hybrid nanocomposite exhibits remarkable performance, achieving 95 % tetracycline degradation under simulated solar irradiation within 30 min (solar simulator AM 1.5, 0.1 W cm^{-2} light intensity). Mechanism studies using optical filters and radical scavengers confirm the role of interfacial charge transfer and reactive oxygen species in the photocatalytic process. The catalyst maintains its activity over four consecutive cycles, highlighting its potential for practical applications in sustainable water remediation.

1. Introduction

The contamination of water resources by pharmaceutical residues has become one of the most pressing environmental challenges of the past decade. Among them, tetracycline antibiotics (TC) are of particular concern due to their widespread use in human and veterinary medicine, their chemical stability, and their persistence once released into natural ecosystems [1]. These compounds enter aquatic systems primarily through excretion, agricultural runoff, and improper disposal. Their resistance to natural degradation processes [2] and poor removal efficiency in conventional wastewater treatment plants [3] result in their continuous accumulation in surface and groundwater. Such persistence not only disrupts microbial communities and nutrient cycling [4] but also fosters the development and dissemination of antibiotic-resistant bacteria, representing a serious ecological and public health risk [5]. Consequently, there is a strong need for innovative remediation technologies capable of ensuring both efficiency and sustainability [6].

Among the strategies currently under investigation, photocatalysis has emerged as a particularly promising approach for the degradation of persistent organic contaminants [7–9]. This process relies on the excitation of a photocatalyst under light irradiation, generating electron–hole pairs that trigger the formation of reactive oxygen species (ROS), which subsequently oxidize and mineralize pollutants [10,11]. Carbon-based nanomaterials, and in particular carbon dots (CDs), are of growing interest because of their unique set of advantages: high water dispersibility, tunable surface functionalities, remarkable photoluminescence, and biocompatibility [12,13]. These properties make them suitable candidates for environmental applications, including pollutant degradation and sensing.

These features make CDs highly versatile platforms for photocatalytic and sensing applications. Importantly, their photocatalytic activity can be significantly enhanced when combined with plasmonic metals such as silver, which act as electron sinks and improve light harvesting through localized surface plasmon resonance. This synergy accelerates charge separation and increases ROS generation, resulting in more efficient pollutant degradation [14–16].

* Corresponding author at: Department of Cultural Heritage, University of Salento, Via D. Birago 64, Lecce, 73100, Italy.
E-mail address: gabriele.giancane@unisalento.it (G. Giancane).

https://doi.org/10.1016/j.surfin.2025.107873
Received 22 July 2025; Received in revised form 2 September 2025; Accepted 14 October 2025
Available online 15 October 2025

Sustainability also plays a pivotal role in the design of next-generation photocatalysts. Recent studies have demonstrated that biomass waste can serve as an abundant and renewable precursor for the synthesis of CDs, thus aligning material development with green chemistry and circular economy principles. For example, food and agricultural residues such as coffee waste or silverskin can be transformed into carbon nanomaterials with heteroatom functionalities that further enhance photocatalytic performance [17–19]. This approach not only reduces the environmental impact of waste disposal but also creates added value materials, contributing to resource efficiency [20,21]. Herein, we report a rapid, low-cost, and sustainable microwave-assisted synthesis of Ag-decorated carbon nanoparticles (MWCNPs@Ag) using spent coffee grounds as the carbon precursor. This waste-derived feedstock introduces heteroatom functionalities into the carbon framework, which are known to promote charge transfer processes and enhance photocatalytic activity [19–21]. The hybrid nanocomposite benefits from the synergistic coupling between the carbonaceous component and the silver nanoparticles, which exhibit strong plasmonic features and interfacial Ag···O bonding interactions [22,23]. In this study it has been further developed to impart interesting photocatalytic properties to the resulting system. As will be described in detail, the system effectively degrades tetracycline in aqueous solution without the need for any additional chemical agents, relying solely on light stimulation [23].

These features enable efficient light-driven tetracycline degradation under mild condition, without the need for additional oxidants or harsh reaction conditions.

Considering some of the most recent and performing photocatalytic systems reported for tetracycline degradation (Table S1), based on semiconductor heterojunctions and oxide–sulfide composites, they typically reach removal efficiencies above 85–95 % under visible or solar irradiation [24–33]. Within this framework, the MWCNPs@Ag nanostructures developed in this work display a particularly competitive performance, achieving 95 % degradation in only 30 min under simulated solar light. This positions our material in the upper range of the most efficient photocatalysts reported to date, while offering the additional advantage of a rapid and sustainable synthetic route based on waste valorization.

The exceptional photocatalytic performance, combined with the ultra-fast and scalable synthesis method, makes this material a highly promising candidate for practical water remediation applications, while simultaneously exemplifying the valorization of biomass waste within a circular economy framework.

2. Results and discussion

2.1. Spectroscopic characterization and formation mechanism of CNPs/Ag nanocomposites

The structural and chemical transformations occurring during the microwave-assisted synthesis of silver-functionalized carbon nanoparticles (MWCNPs@Ag) were thoroughly investigated through a multi-technique spectroscopic approach. Beginning with the pristine CNPs derived from spent coffee grounds, the initial characterization revealed fundamental insights into the starting material properties. UV–Visible spectroscopy (Fig. 1a) displayed a completely featureless absorption profile across the measured wavelength range, with no observable distinct peaks or shoulders. This monotonic absorption behaviour is characteristic of highly disordered carbonaceous materials lacking

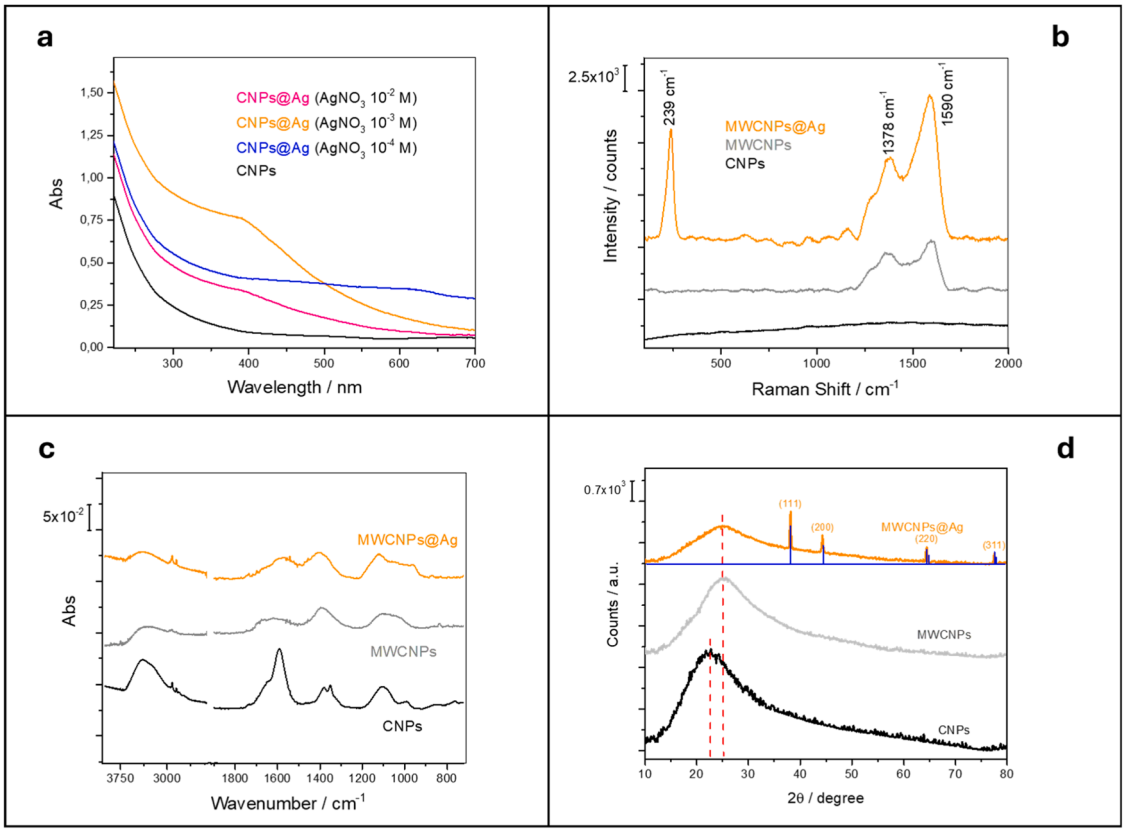

Fig. 1. a) Absorption spectra of CNPs exposed to microwave stimulus in presence of different $AgNO_3$ concentrations in the range 220–700 nm. b) Raman vibrations (200–2000 cm^{-1}) of the CNPs, MWCNPs and MWCNPs@Ag deposited by drop-cast on a silicon support. c) FTIR spectra of the three nanosystems directly casted onto the ATR IRE element. d) XRD pattern recorded for CNPs, MWCNPs, and MWCNPs@Ag over the 10–80° 2θ range. The signals of Ag nanoparticles according to JPCS file No 04–0783 are reported in blue. For clarity, the positions of the signals discussed in the text are indicated on both the Raman spectrum (panel b) and the XRD profile (panel d).

extended π-conjugation systems [34]. Complementarily, Raman spectroscopy analysis (Fig. 1b) further confirms the amorphous nature of the untreated CNPs, with spectrum showing complete absence of the characteristic D and G bands typically associated with graphitic carbon structures [35]. The missing Raman signatures indicate that the initial carbon matrix possesses neither crystalline graphite domains nor significant defect structures that would give rise to these vibrational modes. Fourier-transform infrared (FTIR) spectroscopy (Fig. 1c) provides crucial information about the surface chemical functionality of the as-prepared CNPs. The spectra exhibited several prominent absorption bands corresponding to oxygen-containing functional groups that decorate the carbon nanoparticle surfaces. A broad, intense band centred at 3400 cm^{-1} has been attributed to stretching vibrations of hydrogen-bonded O–H groups originating likely from surface-adsorbed water molecules and hydroxyl functionalities such as phenols or carboxylic acids. A broad signal around 1600 cm^{-1} is also observed and is typically assigned to a combination of δ(H–O–H) bending and C=C stretching in disordered aromatic clusters. The fingerprint region in the range 1050–1250 cm^{-1} displayed complex overlapping bands from C–O stretching modes associated with alcohols, ethers, and epoxides. This comprehensive FTIR analysis confirms that the starting CNPs possess a highly oxygenated surface rich in polar functional groups, according to previous results [19,36] and suggesting that they can potentially serve as anchoring sites for metal ions.

Microwave irradiation of the CNPs (MWCNPs) at 300 W for 30 s induced a red shift in the spectral drift below 300 nm (Fig. 1a, grey line), suggesting a surface modification of the system, which has been subsequently investigated in more detail. Raman spectroscopy provides further evidence of structural reorganization (Fig. 1b, grey line), with the emergence of two new bands at 1378 cm^{-1} (D band) and 1590 cm^{-1} (G band). The D band originates from disordered sp^2 carbon or graphitic edge sites, while the G band corresponds to in-plane stretching vibrations of ordered sp^2-bonded carbon atoms [37]. The calculated D/G intensity ratio of 0.74 indicates the presence of nanometer-sized graphitic domains embedded within a still largely amorphous carbon network, after microwave irradiation [35,37]. Concurrently, FTIR investigations (Fig. 1c, grey line) reveal substantial changes in surface chemistry following microwave exposure. Most notably, the intensities of both the O–H (3400 cm^{-1}) and the broad ~1600 cm^{-1} bands significantly decreased, suggesting dehydration and partial breakdown of hydrogen-bonded hydroxyl networks. Therefore, a broad band at 1720 cm^{-1}, imputable to carbonyl stretching modes, is observed in the FTIR spectrum of MWCNPs. The region at 1050–1250 cm^{-1} also shows spectral simplification, suggesting a loss or transformation of some C–O–H and C–O–C groups [38]. This behaviour reflects not a simple thermal reduction, but rather a microwave-induced reorganization of surface functionalities, potentially assisted by localized heating and reorganization of the carbon framework [39].

The microwave-assisted incorporation of silver nanoparticles into the CNPs matrix exhibited pronounced concentration-dependent behaviour across the tested $AgNO_3$ range (10^{-4} to 10^{-2} M). UV–Vis spectral evolution (Figs. 1a and S1) revealed that the surface plasmon resonance characteristics varied systematically with precursor concentration. The 10^{-3} M condition produced the most well-defined response, exhibiting a plasmon band centred at about 400 nm (Fig. 1a, orange line). In contrast, the 10^{-4} M sample (magenta line) showed only marginal plasmonic resonance, while the 10^{-2} M treatment resulted in broadened absorption features (blue line) suggesting nanoparticle aggregation. Figure S1 presents the UV–Vis spectra of $AgNO_3$ solutions at varying concentrations (10^{-4} to 10^{-2} M) subjected to microwave treatment without CNPs. The absence of any plasmon resonance features across all concentrations confirms that the carbon matrix is essential for silver nanoparticle formation under these synthetic conditions.

The concentration dependence in the formation of MWCNPs@Ag is manifested in the Raman spectra (Figs. 1b and S2). MWCNPs@Ag prepared with a 10^{-3} M silver nitrate solution exhibit the most pronounced structural modifications. Compared to pristine MWCNPs, the hybrid material shows a lower D/G intensity ratio (0.57) and the exclusive appearance of a distinct band at 239 cm^{-1}, which can be assigned to interfacial Ag···O vibrations [40–43]. This feature is missing in pristine CNPs, in microwave-treated CNPs, and in $AgNO_3$ solutions irradiated without CNPs (Figures S1 and S2), confirming that it arises from a specific interaction between silver nanoparticles and oxygenated functionalities of the carbon matrix. The intermediate concentration of silver thus appears optimal to provide sufficient silver for nanoparticle formation and to preserve the integrity of the carbon framework. Additionally, Raman spectra of 10^{-3} M $AgNO_3$ treated without MWCNPs show only residual nitrate signatures (~1045 cm^{-1}) and no Ag oxidation, confirming that nanoparticle formation requires the carbon substrate.

In addition to the precursor concentration, the microwave irradiation time was also found to be a crucial parameter. At shorter exposure (15 s), no plasmonic resonance was detected, suggesting that silver nanoparticles had not yet nucleated. Conversely, extending the irradiation to 45 s led to vigorous boiling of the aqueous suspension, causing uncontrolled conditions. The intermediate duration of 30 s provided the best compromise, reproducibly yielding well-defined plasmonic features around 400 nm without detrimental thermal effects. This condition was therefore selected as the optimal irradiation time for the synthesis of MWCNPs@Ag. It is worth noting that the proposed approach appears particularly eco-friendly, since in addition to employing waste materials for the preparation of the photocatalytic system, it is also extremely rapid and energy efficient. Furthermore, the instrumental setup used is easily accessible and associated with moderate costs.

X-ray diffraction (XRD) analysis was performed on the three samples CNPs, MWCNPs, MWCNPs@Ag and is reported in Fig. 1d As anticipated by Raman spectroscopy, the CNPs exhibit the typical diffraction pattern of amorphous carbon-based structures, with a broad signal centred around 23.7° [44,45]. Particularly interesting is the behaviour observed in the case of the nanostructures after microwave treatment. The peak initially observed at 23.7° shifts to higher angles, with a maximum centred at 25.2°, characteristic of the (002) plane of graphite, and the signal generally appears less broadened [46]. In the XRD profile of the MWCNPs@Ag composite, the band corresponding to the carbonaceous nanostructures does not appear to be significantly affected by the presence of $AgNO_3$ during the microwave treatment. On the contrary, the characteristic signals of silver nanoparticles emerge at 38.09°, 44.29°, and 64.46° [47], which can be assigned to the (111), (200), and (220) planes of face-centered cubic (FCC) silver nanoparticles (JPCS file No 04–0783). These findings support the results obtained from Raman and UV–Vis analysis, confirming the formation of Ag nanostructures induced by the microwave treatment and the presence of CNPs.

Detailed characterization of the MWCNPs@Ag composite reveals multifaceted interfacial chemistry. The unique 239 cm^{-1} Raman signature points to specific bonding configurations between silver nanoparticles and oxygenated carbon sites, while complementary FTIR analysis (Fig. 1c, orange line) shows concurrent modifications in surface functionality. The enhanced definition of the bands at ~1550 cm^{-1} and ~1400 cm^{-1} is consistent with the asymmetric and symmetric stretching vibrations of deprotonated carboxylate groups (COO^-), suggesting that Ag^+ ions interact selectively with pre-existing carboxylic functionalities on the carbon surface. These groups likely serve as anchoring sites for silver nucleation, ultimately enabling the in situ reduction of Ag^+ to Ag^0 under microwave irradiation. Notably, the complete disappearance of the 1600 cm^{-1} band observed in MWCNPs@Ag implies a profound modification in the local electronic environment and/or a suppression of previously disordered π-domains. The C–O vibrational region also shows changes, likely due to further surface condensation reactions or Ag-assisted structural rearrangement. These observations support a mechanism in which Ag^+ ions are first electrostatically adsorbed onto oxygenated surface groups, and then locally reduced via microwave-activated redox processes, leading to the formation of Ag^0 nanoparticles. Supporting this observation, ζ-potential measurements reveal

that the CNPs exhibit a surface charge of (−27 ± 3) mV. Following microwave treatment, this value decreases to (−32 ± 3) mV, as a result of the surface modifications previously identified in the IR spectrum. A further significant reduction to (−25 ± 8) mV is observed for the MWCNPs@Ag complex, confirming the formation of a supramolecular assembly between the carbon nanostructures and Ag^0.

The role of the microwave stimulus can be ascribed to the formation of dielectric hot spots and localized heating around CNPs, which promote the nucleation and coalescence of Ag nanoparticles [48]. The small size of AgNPs (tens of nm) excludes resonant coupling with microwaves but still enhances local temperature, as confirmed by the violent boiling observed for exposures times longer than 40 s in 10^{-3} M $AgNO_3$/CNPs suspensions (not in controls). The resulting hybrid system exhibits enhanced sp^2 ordering (Raman), reduced surface polarity (FTIR), and clear plasmonic features (UV–Vis). Overall, complementary XRD, Raman, FTIR and TERS data consistently support the reduction of Ag^+ to metallic Ag^0, ruling out the formation of silver oxides, and its selective interaction with oxygenated groups on the CNP surface.

2.2 TERS characterization of the nanocomposites

The nanostructures have been morphologically characterized using TERS analysis [49]. The choice of this approach, less conventional than others previously reported in the literature, lies in the wealth of chemical, not only dimensional, information that can be obtained through this analysis. In fact, beyond outlining the classical morphological profile via AFM, it is also possible to map the sample in detail using tip-enhanced Raman spectroscopy.

The spectroscopic data collected during the already reported synthesis phase, indicate that the ratio between the G and D bands of the carbonaceous fragment of the nanostructures changes before and after microwave treatment. Furthermore, the interaction between the carbonaceous component and the metallic part is evidenced by the appearance of a distinct signal at 239 cm^{-1}, attributable, as previously described, to the formation of an Ag···O bond. The spectral position of these peaks, being well-separated, allowed for a clear mapping of the sample: the signal at 516 cm^{-1}, corresponding to the silicon substrate where the samples were deposited by dip-coating, is denoted in blue; the G band of the carbonaceous structure, centered at 1590 cm^{-1}, is marked in red; and the stretching vibration of the Ag···O bond, at 239 cm^{-1}, is mapped in green. In Figure S3, the AFM map of the pristine CNPs nanostructures clearly shows small structures on the order of 40 nm, confirming previous observations of analogous structures [19]. Unfortunately, CNPs do not exhibit significant Raman features, making it impossible to extract useful information about this system through TERS. In Fig. 2, TERS technique was employed to investigate both MWCNPs and MWCNPs@Ag, from morphological and spectroscopic point of view.

The dimensions of MWCNPs appear to differ significantly from those observed prior to microwave treatment. Specifically, the size of the carbon nanoparticles ranges between 15 and 25 nm, which is smaller than that of the untreated CNPs. Notably, as also confirmed by Raman measurements, the MWCNPs, clearly visible in red (Fig. 2a), exhibit a characteristic Raman spectrum of carbon-based structures, with the D and G bands centered at 1380 and 1590 cm^{-1} (Fig. 2a'). TERS analysis further reveals the structure of the MWCNPs@Ag nanocomposites

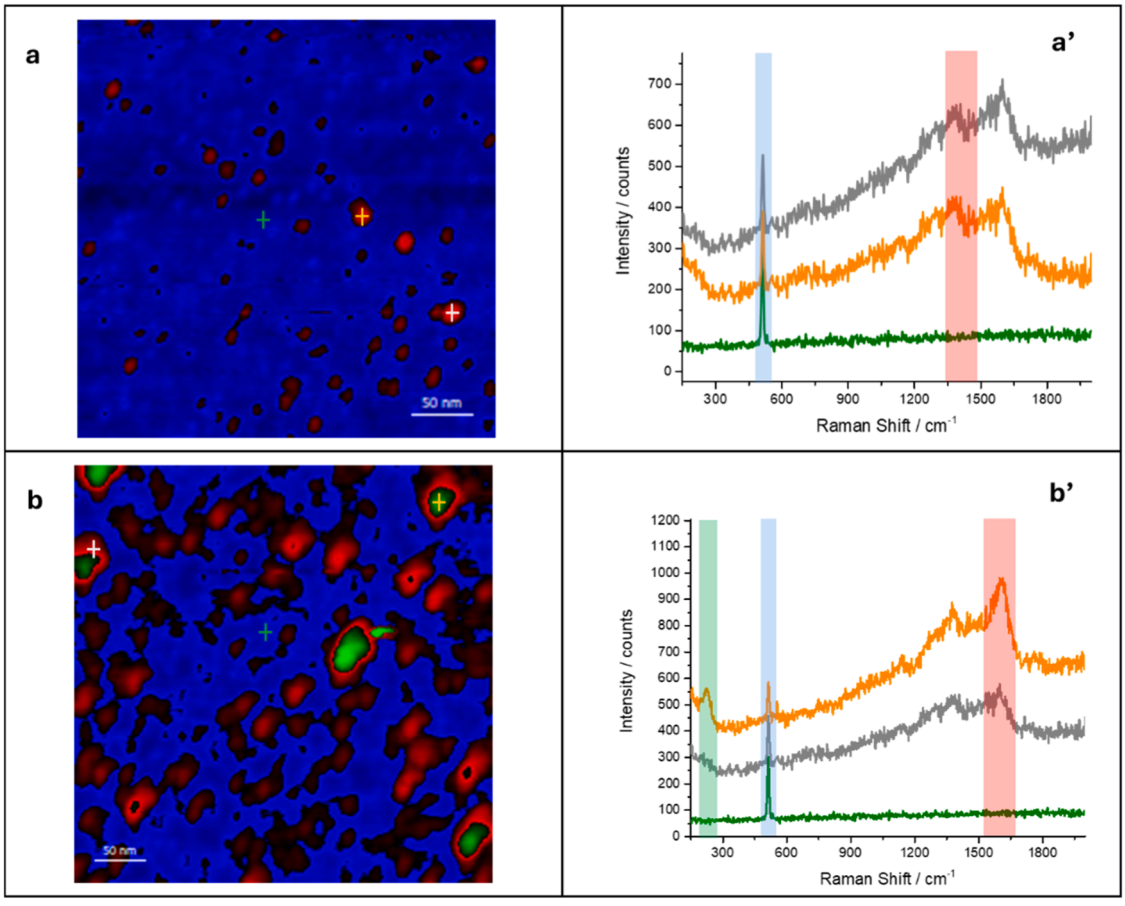

Fig. 2. TERS analysis performed on dip-coated films of MWCNPs and MWCNPs@Ag (panels a and b, respectively). The signal localized at 516 cm^{-1}, attributed to silicon, is shown in blue for both samples, while the signal at 1590 cm^{-1}, due to the G band of carbonaceous structures, is mapped in red. Additionally, in panel b only, the signal at 240 cm^{-1}, associated with Ag···O vibrations, is mapped in green. Raman spectra ascribable to the points marked with color-coded crosses on the hybrid spectroscopic/morphological images are shown in panels a' and b'.

(Fig. 2b). In addition to the blue colour, corresponding to the silicon peak from the substrate where the hybrid is deposited, green regions are observed (related to the peak at 239 cm^{-1}, previously attributed to the formation of an Ag···O bond), with dimensions around 30 nm. These are surrounded by a red halo that, as in the case of the MWCNPs, corresponds to the Raman mapping signal centered at 1590 cm^{-1}, which is attributed to the stretching vibrations of sp^2-hybridized carbon–carbon bonds in the carbonaceous matrix. Importantly, the size of the silver core is consistent with the position of the plasmonic peak at 400 nm, while the carbonaceous component appears as an organic "shell" surrounding the metal, formed during synthesis [23]. The size, shape, and morphology of the hybrid MWCNPs@Ag structure are confirmed by TEM images, in which the metallic nanostructures are particularly evident (Figure S4).

Further investigation of the size distribution of CNPs, MWCNPs, and MWCNPs@Ag was performed using a nanoparticle tracking analyzer with three-laser illumination, directly in aqueous suspension (Figure S5). This analysis confirms that microwave treatment reduces the size of the nanostructures, from 45 ± 6 nm to 25 ± 12 nm for CNPs and MWCNPs, respectively, while the hybrid MWCNPs@Ag reaches a size of 43 ± 9 nm, in full agreement with the morphology observed via atomic force microscopy (Figure S6).

2.3. *Photocatalytic behavior of CNPs, MWCNPs, and MWCNPs@Ag toward tetracycline degradation*

The three systems, CNPs, MWCNPs, and MWCNPs@Ag were incubated in aqueous solution in the dark in the presence of tetracycline (TC) at a concentration of 10^{-4} M. The UV–Vis absorption spectra of TC were monitored in the range of 600–250 nm, with particular attention to the absorbance bands at 365 nm and 270 nm, to evaluate the potential impact of the nanocomposites on the stability of tetracycline.

Consistent with literature reports, carbon nanoparticles (CNPs) exhibit redox activity capable of inducing redox reactions [36,50]. In this context, under dark conditions, CNPs slightly reduce the TC concentration by approximately 3 % after 10 min and by 7 % after 30 min (Figure S7). Comparable behavior was observed with MWCNPs, indicating that despite the structural modifications induced by microwave processing, the interaction with TC follows a similar redox degradation pathway. Specifically, the absorbance signal at 365 nm suggests that about 3 % of TC is degraded in the presence of MWCNPs after 10 min in the dark, increasing to 9 % after 30 min (Figure S7). In contrast, the MWCNPs@Ag system exhibits a different behavior: when exposed to the same dark conditions, no appreciable change in the TC absorption spectrum is observed for up to 30 min. This behavior can be ascribed to the passivation of oxygenated surface groups, which in pristine CNPs act as electron-transfer sites. FTIR spectra reveal the evolution of carboxylate vibrations upon Ag incorporation, while Raman analysis highlights the exclusive 239 cm^{-1} band, both evidencing the formation of Ag···O bonds. Similar mechanisms, where carboxylate groups mediate Ag^+ coordination and nanoparticle formation, have been reported in the literature [51,52]. Such interfacial interactions stabilize the redox-active functionalities of the carbon matrix, suppressing TC reduction in the dark.

Before starting the experiment upon light irradiation, the photostability of the developed nanocomposites, CNPs, MWCNPs, MWCNPs@Ag were checked keeping them under gentle stirring and solar-simulated illumination for 30 min in the same conditions of the photocatalytic experiments (see Experimental Section). No change in the UV–Vis spectra was detected confirming the stability of the catalysts.

Under solar-simulated illumination, the photochemical behavior of the three systems changes significantly. The CNPs-TC solution shows only slightly higher degradation capacity if compared to the dark condition (Fig. 3a). This implies that photoexcitation has a little impact on

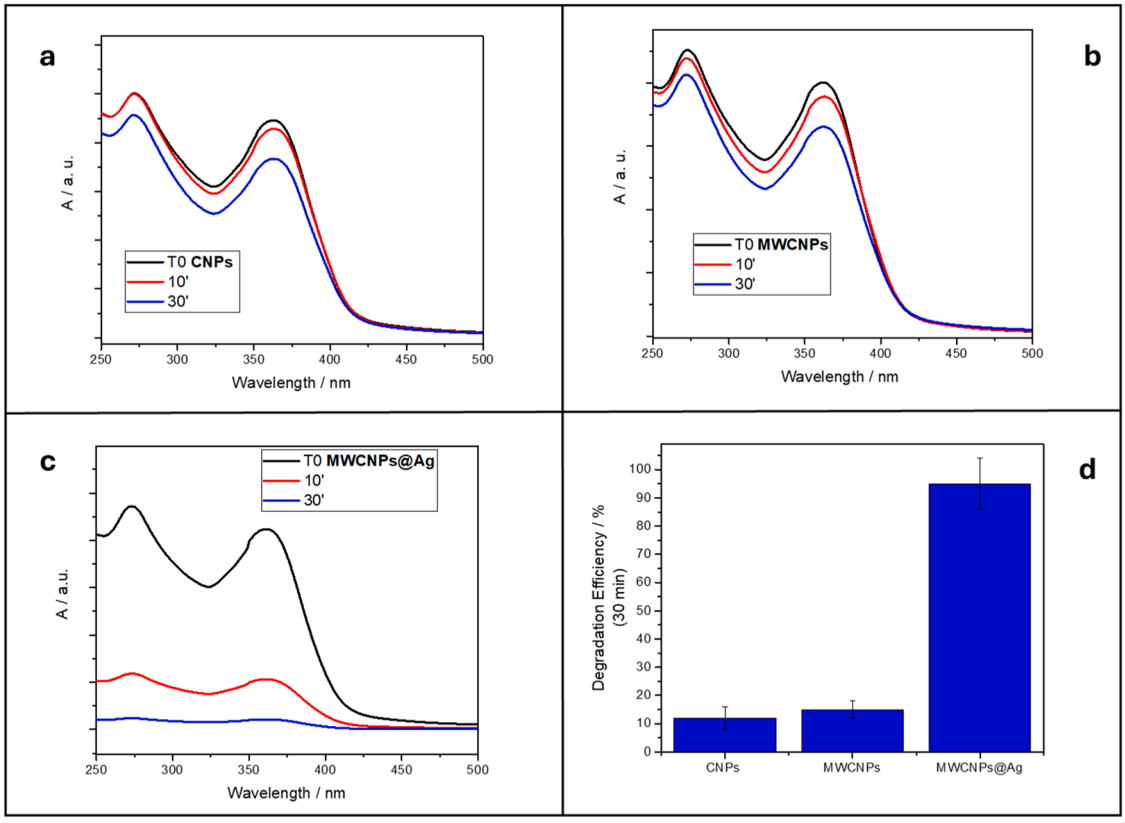

Fig. 3. Photocatalytic activity of CNPs (a), MWCNPs (b), and MWCNPs@Ag (c) on an aqueous TC solution (10^{-4} M) under light exposure. (d) Summary histogram of TC degradation efficiencies for the three systems after 30 min of illumination.

the photocatalytic degradation of TC by pristine CNPs.

Similar behavior is observed for MWCNPs under illumination, further confirming their limited photocatalytic efficiency under these conditions (Fig. 3b). However, the MWCNPs@Ag system exhibits a dramatically enhanced photocatalytic response. Within just 10 min of light illumination, the concentration of TC in solution decreases by approximately 75 %, reaching an impressive 95 % degradation after 30 min (Figs. 3c and 3d, respectively). This striking performance suggests the occurrence of efficient electronic communication between the organic and inorganic components of the MWCNPs@Ag hybrid, promoting the generation of reactive radical species responsible for TC degradation. Considering the simultaneous bleaching of both absorption maxima of TC, it is possible to hypothesize that the photodegradation of the molecule involves the entire backbone of the molecule [11]. Structural investigations (XRD, Raman/TERS, FTIR) confirm the formation of Ag nanoparticles in intimate contact with the carbon matrix and highlight specific interfacial interactions. These results are consistent with the observed photocatalytic behavior, supporting the idea that the Ag–carbon interface plays a key role in the enhanced degradation efficiency of the hybrid system.

To further clarify the photocatalytic kinetics, the degradation of TC catalyzed by MWCNPs@Ag was analyzed according to a pseudo-first-order model (Figure S8). The reaction follows the equation $\ln\frac{A_0}{A} = -k_{obs}t$ where k_{obs} is the observed rate constant, and t is the irradiation time. From the fitting, a rate constant of $k_{obs} = 0.099$ min^{-1} was obtained, corresponding to a half-life time of $t_{1/2} = 7.001$ min (calculated as $\ln 2/k_{obs}$). These values highlight the high photocatalytic efficiency of the MWCNPs@Ag system, in agreement with the degradation percentages reported in Fig. 3. The pseudo-first-order behavior also explains the faster degradation observed in the initial stages, when the TC concentration is higher, followed by a slower removal rate after 30 min.

To investigate the mechanism of light-induced charge transfer, a series of optical filters were employed to isolate specific energy ranges and assess their roles in the photocatalytic process. A long-pass optical filter with a cutoff at 360 nm was used. Under these conditions, the degradation of TC was comparable to that observed in the dark (Fig. 4a), with degradation efficiencies reaching 7 % at 30 min. This suggests that the Ag nanostructures do not exhibit plasmon-driven photoactivity in the degradation of TC, and that any significant electron transfer from Ag to MWCNPs is unlikely. Interestingly, the slightly higher degradation rate observed with the 360 nm cutoff filter, compared to dark conditions, can be attributed to the residual absorption capability of MWCNPs as evident from the UV–Vis spectrum of the MWCNPs@Ag.

The role of Ag nanoparticles was further investigated using a short-pass filter allowing photon transmission below 380 nm. Under these conditions, significant TC degradation was observed in the presence of MWCNPs@Ag, approximately 20 % after 10 min and 80 % after 30 min (Fig. 4b), values only slightly lower than those obtained under full-spectrum white light illumination. These results, combined with the negligible photocatalytic activity of MWCNPs alone, suggest that the excitation of carbonaceous structures leads to electron promotion from the HOMO to the LUMO of the MWCNPs, followed by charge transfer to the Ag nanostructures [53].

It can thus be proposed that Ag nanostructures act as electron sinks, effectively enhancing exciton separation and facilitating the availability of electrons and holes for radical formation, ultimately leading to efficient TC degradation. To further elucidate the photocatalytic mechanism, scavenger experiments were performed using Coenzyme Q0 (Q0) and triethanolamine (TEA) as electron and hole scavengers, respectively. Both agents were added to the reaction system at a final concentration of 1 mM under simulated solar irradiation. The presence of these scavengers led to a substantial reduction in degradation efficiency after 30 min: approximately 40 % in the presence of Q0 and 30 % in the presence of TEA (Fig. 4c). These findings confirm that both photogenerated electrons and holes play critical roles in the photocatalytic process, with holes (h^+) likely having a slightly more dominant contribution to the overall degradation pathway.

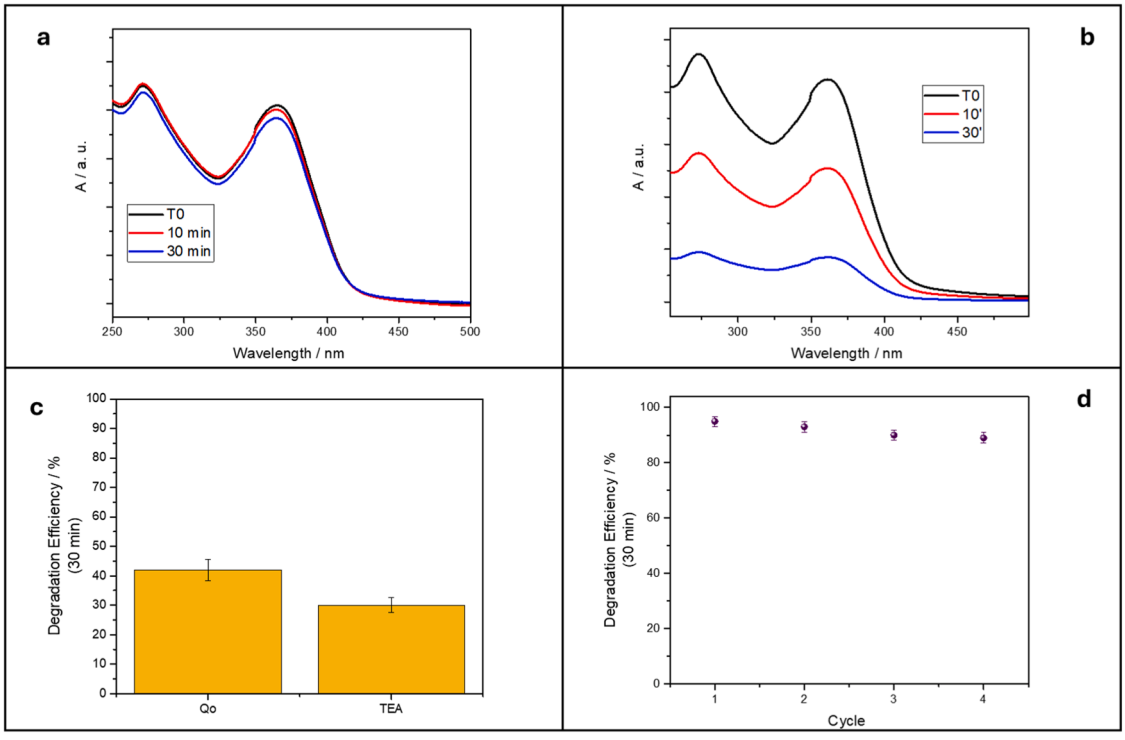

Fig. 4. (a) Degradation of TC in the presence of MWCNPs@Ag using an optical filter excluding radiation in the 220–370 nm range ($T_o = 0$ min of light exposure). (b) Degradation of TC in the presence of MWCNPs@Ag using a filter excluding radiation for $\lambda > 400$ nm. (c) Photodegradation percentage using the full spectral range of the solar simulator in the presence of two scavengers: Coenzyme Q_o (Q_o) and triethanolamine (TEA). (d) Degradation efficiency of the same catalyst over four consecutive cycles (30 min each cycle).

On the basis of the scavenger tests (Fig. 4c), the more pronounced suppression of photocatalytic activity in the presence of TEA suggests that photogenerated holes (h^+) are the dominant oxidative agents. It can be reasonably supposed that h^+ may also lead to the generation of hydroxyl radicals (·OH) through oxidation of adsorbed water or hydroxide ions. In parallel, the interfacial charge transfer from MWCNPs to Ag nanoparticles could favor the reduction of dissolved oxygen, thus potentially generating superoxide radicals ($O_2{\cdot}^-$). Therefore, even though experimental confirmation is lacking, we may hypothesize that the overall degradation mechanism involves both direct oxidation by h^+ and indirect oxidation mediated by subsequent reactive oxygen species (ROS), mainly ·OH and $O_2{\cdot}^-$. This interpretation is consistent with previously reported behaviors in carbon/metal hybrid photocatalysts [11, 15,16,53], and further supports the proposed mechanism involving photo-induced charge separation, interfacial electron transfer between MWCNPs and Ag nanoparticles, and ROS formation responsible for tetracycline degradation.

The reusability of the MWCNPs@Ag nanocomposite was evaluated over four consecutive photocatalytic cycles to assess its stability and long-term performance in tetracycline degradation. In each cycle, the photocatalyst was recovered by centrifugation, washed thoroughly with deionized water, and reused under identical experimental conditions. Remarkably, no significant loss in photocatalytic efficiency was observed across all cycles, both under short (10 min) and extended (30 min) irradiation periods (Fig. 4d and S9). After each cycle, the degradation efficiency remained at about 70 % at 10 min and 90 % at 30 min, indicating excellent structural stability and sustained photoactivity of the hybrid material. No appreciable structural or optical modifications were detected in the recovered MWCNPs@Ag catalyst. In particular, FTIR spectra and UV–Vis absorption profiles recorded before and after recycling (four cycles at 30 min) were essentially identical (Figure S10), confirming that the surface functionalities and plasmonic properties remain unaltered. These findings highlight the robustness of the system, corroborate the photocatalytic results reported in Fig. 4d, and confirm that the MWCNPs@Ag nanostructures maintain their functional integrity and reactive surface characteristics over repeated use, making them highly promising candidates for practical water treatment applications.

3. Experimental sections

3.1. Chemicals

Tetracycline (TC) (≥ 98.0 %, HPLC), $AgNO_3$ (≥ 99.0 %, ACS reagent), triethanolamine (TEA) (98.0 %, reagent grade) and Coenzyme Q0 (Q0) (≥ 98.0 %, HPLC) were purchased from Merck and utilized in this study without any further modifications. Ultrapure water (18.2 MΩ·cm at 25 °C) was used in all the experiments.

3.2. Synthesis and characterization of nanocomposites based on CNPs and AgNPs

Nanocomposites based on CNPs and AgNPs (MWCNPs@Ag) were synthesized using a simple and ultra-fast method, employing a microwave oven designed for domestic use. In a typical experiment, a solution containing 0.2 mL of $AgNO_3$ (5×10^{-2} M), 2 mL of previously synthesized CNPs [19], and 0.2 mL of ultrapure water was prepared. The resulting solution was then placed in a domestic microwave oven for 30 s at 300 Watts. The nominal power output of 300 W, as specified by the manufacturer, was used without further calibration. It is worth noting that the reproducibility of the MWCNPs@Ag synthesis strongly depends on the reaction volume and vessel geometry. In particular, volumes above ~15 mL in narrow and deep beakers result in less efficient yields, most likely due to non-uniform heating when using a domestic microwave oven. Subsequently, the obtained nanostructures were allowed to cool to room temperature for 30 min before being used in subsequent experiments. The carbon nanoparticles were also subjected to treatment in the microwave oven in the absence of the silver nitrate solution to perform a control test.

The synthesized nanostructures (CNPs, MWCNPs and MWCNPs@Ag) were characterized using various spectroscopic techniques. UV–Vis absorption measurements were carried out using a Cary-5000 spectrophotometer. Visible and near UV filters were purchased by Edmund Optics.

Fourier transform Infrared (FTIR) spectroscopy was performed by means of a Spectrum One spectrophotometer (PerkinElmer, Waltham, MA, USA) equipped with a triglycine sulfate (TGS) detector and operating in ATR mode in the 4000–600 cm^{-1} frequency range. The IRE was a three-bounce diamond microprism with a 4 mm diameter. For spectra acquisition 3 μL aliquots of samples were layered onto the IRE and left drying at the air. Each spectrum is obtained as an average of 32 interferograms.

Raman investigations were conducted using Horiba Xplora microRaman. Dip-coating method was used to transfer three layers of CNPs, MWCNPs and MWCNPs@Ag respectively on silicon substrates, with an immersion/emersion speed of 1 mm min^{-1}. The samples were irradiated by a 532 nm laser source at a power of 0.125 $mWcm^{-2}$. Each spectrum was acquired with 30 scans in the 150–2000 cm^{-1} range.

The Tip Enhanced Raman Spectroscopy (TERS) analyses were performed by an SmartSPM 1000 AIST-NT coupled to a Horiba Xplora microRaman by an optical bridge. A TERS (Tip-Enhanced Raman Spectroscopy) system utilizes a silver AFM tip to concentrate the incident light at its apex. The tip functions as a nanoscale light source and local field enhancer, significantly increasing Raman sensitivity while confining the probed volume to the nanoscale region directly under the tip. The excitation wavelength of the used laser was 638 nm.

TEM analyses were performed using a JEOL JEM 1400 microscope operating at 80 kV and equipped with a Lanthanum hexaboride (LaB6) electron source. For sample preparation, MWCNPs@Ag suspensions were sonicated in water for 20 min in an ultrasonic bath. Subsequently, a drop of the resulting dispersion was deposited onto carbon-coated copper grids, left to dry under ambient conditions, and finally placed in an oven at 50 °C to ensure complete removal of residual water.

Powder X-ray diffraction (XRD) patterns were collected using a Malvern Panalytical Aeris diffractometer operating in transmission geometry. The instrument was equipped with a PIXcel3D solid-state detector and a copper anode X-ray source (Cu $K\alpha_1$: 1.5406 Å; Cu $K\alpha_2$: 1.5444 Å). Data were acquired over a 2θ range of 10° to 80°, with a scan rate of 0.013°/s.

CNPs, MWCNPS and MWCNPS@Ag ζ-potential measurements were carried out by means of a Malvern Panalytical Nano ZS Zetasizer instrument (Malvern Panalytical Limited, Malvern, U.K.).

CNPs, MWCNPS and MWCNPS@Ag dimensions in aqueous solutions were further investigated by means of a visual multispectral particle analyzer (ViewSizer 3000, Horiba).

3.3. Photodegradation experiments

For the tetracycline (TC) photodegradation experiments, a LOT-Oriel Solar S Class A solar simulator (0.1 W cm^{-2} light intensity) was used. In a typical experiment, 300 μL of a suspension of CNPs, MWCNPs, or MWCNPs@Ag were added to a 10^{-4} M TC solution, giving a final volume of 4.5 mL. To allow adsorption–desorption equilibrium, the suspension was magnetically stirred in the dark for 15 min. The TC absorption band at 350 nm was monitored every 5 min during this period, showing negligible variation in intensity.

Photodegradation was then initiated by placing the beaker containing the photocatalyst solution perpendicularly 10 cm from the light source. At selected time intervals (10 and 30 min), ~1.5 mL aliquots were collected and centrifuged at 2700 rcf for 5 min to separate the solid photocatalyst from the solution. The resulting supernatant was analyzed spectrophotometrically.

To investigate the degradation mechanism, the same experiments

were performed in the dark (after the 15 min equilibration) and using optical filters in combination with the solar simulator. All photocatalytic experiments were conducted at room temperature (18–20 °C). TC degradation efficiency was calculated as $\frac{A_0-A}{A_0} \times 100$, where A_0 is the absorbance value at 365 nm at the starting point, after the 15 min equilibration, and A is the absorbance value at each time point.

To study the mechanism underlying the photodegradation process of tetracycline, photocatalytic degradation measurements of the MWCNPs@Ag nanostructures were also conducted in the presence of two scavenger species, triethanolamine and Coenzyme Q0 in two different experiments. Therefore, Coenzyme Q0 (as an electron scavenger) and triethanolamine (as a hole scavenger), at a final concentration of 1 mM, were added to the reaction's solution during the photocatalytic experiments.

The recycling experiments were performed for four consecutive cycles to test the stability and reusability of synthetized material. After each cycle, the photocatalyst was separated by centrifugation, washed thoroughly with deionized water, and then reused for the next steps.

4. Conclusions

In this study, we developed a sustainable and ultra-fast microwave-assisted synthesis route for the preparation of silver-decorated carbon nanoparticles (MWCNPs@Ag), employing spent coffee grounds as the carbon precursor. This approach aligns with the principles of green chemistry and the circular economy by transforming food industry waste into functional nanomaterials with high environmental value. Although a full life-cycle or cost analysis is beyond the scope of this study, the reuse of coffee waste as a carbon precursor already represents an intrinsically sustainable and low-cost strategy, as it valorizes an abundant residue otherwise discarded. Future studies could further quantify these benefits through dedicated LCA and economic analyses. The integration of silver nanoparticles within the carbon matrix was achieved within 30 s of microwave irradiation, demonstrating the feasibility of a time-efficient and scalable fabrication process. Comprehensive spectroscopic and structural analyses, including UV–Vis, FTIR, Raman, TERS, and XRD, provided detailed insight into the physicochemical transformations induced by the microwave process and Ag incorporation. Notably, TERS mapping revealed the nanoscale spatial organization of the hybrid system, highlighting the intimate contact between the silver and carbon phases and the formation of interfacial Ag···O bonds. These interactions are essential in modulating the optical and electronic properties of the composite, and ultimately in driving its superior photocatalytic performance. The synthesized MWCNPs@Ag nanostructures exhibited remarkable photocatalytic activity under simulated solar light, achieving 95 % degradation of tetracycline within 30 min, far exceeding the performance of pristine or microwave treated carbon nanoparticles alone. Mechanistic studies using optical filters and selective radical scavengers provided strong evidence for a photo-induced charge transfer mechanism, where excitation of the carbonaceous component promotes electron injection into the Ag nanoparticles. The subsequent generation of reactive oxygen species (ROS) facilitates the oxidative breakdown of the antibiotic molecule, as confirmed by the rapid bleaching of both major absorption bands of TC. The system also demonstrated excellent chemical stability and reusability across four consecutive photocatalytic cycles without significant loss of activity, underscoring its potential for real-world water treatment applications. This robustness, combined with low-cost raw materials, minimal energy input, and environmentally benign synthesis, positions the MWCNPs@Ag hybrid as a highly promising candidate for scalable implementation in the remediation of pharmaceutical contaminants in water. Looking ahead, this work opens avenues for further exploration of waste-derived carbon nanomaterials functionalized with plasmonic or redox-active metals.

CRediT authorship contribution statement

S. Bettini: Writing – review & editing, Supervision, Methodology, Conceptualization. **R. Pagano:** Writing – original draft, Methodology, Conceptualization. **M. Ottolini:** Methodology, Investigation. **L. Valli:** Supervision, Funding acquisition, Conceptualization. **G. Giancane:** Writing – review & editing, Supervision, Methodology, Conceptualization.

Declaration of competing interest

The authors declare that they have no known competing financial interests or personal relationships that could have appeared to influence the work reported in this paper.

Acknowledgements

This research was supported by the PRIN 2022 (protocol number 20228YFRNL), by the PRIN PNRR 2022 (protocol number P2022WLAY7) and by the Spoke 9 – Cascade Call under the project NANOCARB: High-surface-area carbon nanostructures as electronic transducers for artificial photosynthesis, funded by PNRR, MISSION 4 - Network 4 Energy Sustainable Transition (CUP B53C22004060006).

Supplementary materials

Supplementary material associated with this article can be found, in the online version, at doi:10.1016/j.surfin.2025.107873.

Data availability

Data will be made available on request.

References

[1] X. Zhang, T. Cai, S. Zhang, J. Hou, L. Cheng, W. Chen, Q. Zhang, Contamination distribution and non-biological removal pathways of typical tetracycline antibiotics in the environment: a review, J. Hazard. Mater. 463 (2024) 132862, https://doi.org/10.1016/j.jhazmat.2023.132862.
[2] F. Ahmad, D. Zhu, J. Sun, Environmental fate of tetracycline antibiotics: degradation pathway mechanisms, challenges, and perspectives, Environ. Sci. Eur. 33 (2021) 64, https://doi.org/10.1186/s12302-021-00505-y.
[3] F. Wang, Z. Wang, Y. Zhao, J. Zhang, Performance of traditional and emerging water-treatment technologies in the removal of tetracycline antibiotics, Catalysts 14 (2024) 269, https://doi.org/10.3390/catal14040269.
[4] J. Antos, M. Piosik, D. Ginter-Kramarczyk, J. Zembrzuska, I. Kruszelnicka, Tetracyclines contamination in European aquatic environments: a comprehensive review of occurrence, fate, and removal techniques, Chemosphere 353 (2024) 141519, https://doi.org/10.1016/j.chemosphere.2024.141519.
[5] B. Bojarski, B. Kot, M. Witeska, Antibacterials in aquatic environment and their toxicity to fish, Pharmaceuticals 13 (2020) 189, https://doi.org/10.3390/ph13080189.
[6] Y. Amangelsin, Y. Semenova, M. Dadar, M. Aljofan, G. Bjørklund, The impact of tetracycline pollution on the aquatic environment and removal strategies, Antibiotics 12 (2023) 440, https://doi.org/10.3390/antibiotics12030440.
[7] R. Abazari, S. Sanati, L.A. Saghatforoush, Non-aggregated divanadium pentoxide nanoparticles: a one-step facile synthesis. Morphological, structural, compositional, optical properties and photocatalytic activities, Chem. Eng. J. 236 (2014) 82–90, https://doi.org/10.1016/j.cej.2013.09.056.
[8] A. Bouafia, S.E. Laouini, O.B. Ali, H. Daoudi, S. Meneceur, H.A. Mohammed, M. Azzi, F. Alharthi, T. Trzepieciński, Bio-inspired synthesis and photocatalytic applications of α-fe$_2$o$_3$@ZnO nanobinary using *Laurus nobilis* Leaf extract: efficient for anionic and cationic dye degradation with reusability studies, Appl. Organom Chemis. 39 (2025) e70119, https://doi.org/10.1002/aoc.70119.
[9] G.G. Hasan, S.E. Laouini, A. Khelef, H.A. Mohammed, M. Althamthami, S. Meneceur, F. Alharthi, S.A. Alshareef, F. Menaa, Efficient treatment of oily wastewater, antibacterial activity, and photodegradation of organic dyes using biosynthesized Ag@Fe3O4 nanocomposite, Bioprocess. Biosyst. Eng. 47 (2024) 75–90, https://doi.org/10.1007/s00449-023-02946-6.
[10] R. Manju, J.J. Samraj, B. Neppolian, Real sample analysis of persistent contaminant abatement via synergistic adsorption and visible-light catalysis in continuous flow reactors, Sep. Purif. Technol. 360 (2025) 131050, https://doi.org/10.1016/j.seppur.2024.131050.
[11] R. Pagano, S. Bettini, M. Ottolini, G. Ciccarella, L. Valli, G. Giancane, Piezo- and photo- responsive ZnO nanostructures for efficient tetracycline water remediation,

Colloids Surf. A: Physicochem. Eng. Asp. 680 (2024) 132626, https://doi.org/10.1016/j.colsurfa.2023.132626.
[12] Z. Wang, R. Changotra, M. Dasog, G. Singh Selopal, J. Yang, Q.S. He, Carbon quantum dots: synthesis via hydrothermal processing, doping strategies, integration with photocatalysts, and their application in photocatalytic hydrogen production, Sustain. Mater. Technol. 44 (2025) e01386, https://doi.org/10.1016/j.susmat.2025.e01386.
[13] S. Bettini, S. Sawalha, L. Carbone, G. Giancane, M. Prato, L. Valli, Carbon nanodot-based heterostructures for improving the charge separation and the photocurrent generation, Nanoscale 11 (2019) 7414–7423, https://doi.org/10.1039/c9nr00951e.
[14] A. Nazir, P. Huo, H. Wang, Z. Weiqiang, Y. Wan, A review on plasmonic-based heterojunction photocatalysts for degradation of organic pollutants in wastewater, J. Mater. Sci. 58 (2023) 6474–6515, https://doi.org/10.1007/s10853-023-08391-w.
[15] S. Chu, M. Sun, Z. Li, H. Wang, F. Miao, Coordination engineering of defective F and N co-doped carbon dots anchored silver nanoparticles for boosting oxygen reduction reaction, J. Alloys. Compd. 1002 (2024) 175256, https://doi.org/10.1016/j.jallcom.2024.175256.
[16] A. Mei, Z. Xu, X. Wang, Y. Liu, J. Chen, J. Fan, Q. Shi, Photocatalytic materials modified with carbon quantum dots for the degradation of organic pollutants under visible light: a review, Environ. Res. 214 (2022) 114160, https://doi.org/10.1016/j.envres.2022.114160.
[17] A.S. Franca, E.P. Basílio, L.M. Resende, C.A. Fante, L.S. Oliveira, Coffee silverskin as a potential ingredient for functional foods: recent advances and a case study with chocolate cake, Foods 13 (2024) 3935, https://doi.org/10.3390/foods13233935.
[18] A. Imran, F. Ahmed, Y.A. Ali, M.S. Naseer, K. Sharma, Y.S. Bisht, A.H. Alawadi, U. Shehzadi, F. Islam, M.A. Shah, A comprehensive review on carbon dot synthesis and food applications, J. Agric. Food Res. 21 (2025) 101847, https://doi.org/10.1016/j.jafr.2025.101847.
[19] S. Bettini, M. Ottolini, M. Coccimiglio, R. Pagano, V. García-Caballero, M. Cano, J. J. Giner-Casares, L. Valli, G. Giancane, Photoinduced and electrochemical applications of carbon-based nanoparticles from spent coffee grounds, J. Phys. Chem. C 128 (2024) 6180–6188, https://doi.org/10.1021/acs.jpcc.3c07290.
[20] G. Redondo-Fernandez, J. Cigales Canga, A. Soldado, J. Ruiz Encinar, J.M. Costa-Fernandez, Functionalized heteroatom-doped carbon dots for biomedical applications: a review, Anal. Chim. Acta 1284 (2023) 341874, https://doi.org/10.1016/j.aca.2023.341874.
[21] G. Yang, C. Wu, X. Luo, X. Liu, Y. Gao, P. Wu, C. Cai, S.S. Saavedra, Exploring the emissive states of heteroatom-doped graphene quantum dots, J. Phys. Chem. C 122 (2018) 6483–6492, https://doi.org/10.1021/acs.jpcc.8b01385.
[22] K. Ramesh, G. Bhagavanth Reddy, M. Noorjahan, Microwave assisted green synthesis of palladium nanoparticles using dragon fruit peel extract for catalytic reduction of 4-nitrophenol and methylene blue, Reac. Kinet. Mech. Cat. 137 (2024) 2133–2145, https://doi.org/10.1007/s11144-024-02652-8.
[23] B.R. G, R. Dadigala, R. Bandi, K. Seku, K. D, G. Mangatayaru K, A.E. Shalan, Microwave-assisted preparation of a silver nanoparticles/N-doped carbon dots nanocomposite and its application for catalytic reduction of rhodamine B, methyl red and 4-nitrophenol dyes, RSC. Adv. 11 (2021) 5139–5148, https://doi.org/10.1039/d0ra10679h.
[24] J. Liu, Z. Ding, D. Gao, L. Liu, Synthesis and photocatalytic performance of BiOI/ZnO composites for tetracycline degradation and antibacterial applications under visible light irradiation, Mater. Res. Bull. 194 (2026) 113714, https://doi.org/10.1016/j.materresbull.2025.113714.
[25] A.H. Zyoud, Photodegradation of aqueous tetracycline using CuS@TiO_2 composite under solar-simulated light: complete mineralization, catalyst efficiency, and reusability, Heliyon. 11 (2025) e41662, https://doi.org/10.1016/j.heliyon.2025.e41662.
[26] B.S. Subasi, T. Hayri-Senel, E. Kahraman, S. Sezer, G. Nasun-Saygili, N. Erdol-Aydin, Photocatalytic degradation of tetracycline from aqueous solution with graphene oxide and hydroxyapatite composites, Sci. Rep. 15 (2025) 25894, https://doi.org/10.1038/s41598-025-11502-z.
[27] K. Zhu, L. Ma, J. Duan, Z. Fang, Z. Yang, Photocatalytic degradation of tetracycline hydrochloride using TiO2/CdS on nickel foam under visible light and RSM–BBD optimization, Catalysts. 15 (2025) 113, https://doi.org/10.3390/catal15020113.
[28] R. Guo, Y. Zhong, B. Wang, L. Li, W. Qin, Y. Tan, Z. Zhao, N. Liu, Z. Mo, Efficient photocatalytic degradation of tetracycline and its derivatives by green recyclable PAN/Bi2WO6/Cu2O nanofiber membrane, Sep. Purif. Technol. 358 (2025) 130239, https://doi.org/10.1016/j.seppur.2024.130239.
[29] T.L. Yusuf, O.C. Olatunde, D. Masekela, O.D. Saliu, K.D. Modibane, D. C. Onwudiwe, Interfacial S-scheme charge transfer in $MgIn_2S_4$ /ZnO heterojunction for enhanced photodegradation of tetracycline and efficient water splitting, Nanoscale Adv. 7 (2025) 4876–4885, https://doi.org/10.1039/D5NA00573F.
[30] M. Jiang, J. Luo, M. Qiu, K. Peng, G. Wang, Y. Wang, X. Chen, Y. Wu, W. Liu, Enhanced tetracycline removal via Z-scheme activation by a novel magnetic ZnO/Fe3O4-modified biochar, BioMass BioEnergy 200 (2025) 108042, https://doi.org/10.1016/j.biombioe.2025.108042.
[31] Y. Zhang, X. Bo, T. Zhu, W. Zhao, Y. Cui, J. Chang, Synthesis of TiO2-ZnO n-n heterojunction with excellent visible light-driven photodegradation of tetracycline, Nanomaterials 14 (2024) 1802, https://doi.org/10.3390/nano14221802.
[32] S. Thakur, V. Mutreja, A. Tomar, S. Nainwal, K. Kaur, R. Kaur, Q. Li, F.S. Ataya, Phytochemical-assisted fabrication of ZrO2/ZnO nanocomposites: a sustainable approach for efficient photodegradation of tetracycline hydrochloride, J. Mol. Struct. 1330 (2025) 141350, https://doi.org/10.1016/j.molstruc.2025.141350.
[33] A. Panchakeaw, S. Nonthing, R. Dulyasucharit, S. Nanan, Improved photocatalytic activity of magnetically separable Fe3O4/ZnO photocatalyst for complete sunlight-active removal of tetracycline antibiotic, Chem. Phys. Lett. 862 (2025) 141868, https://doi.org/10.1016/j.cplett.2025.141868.
[34] R. Jelinek, Characterization and physical properties of carbon-dots, in: Carbon Quantum Dots, Springer International Publishing, Cham, 2017: pp. 29–46. https://doi.org/10.1007/978-3-319-43911-2_3.
[35] R. Yuan, Y. Guo, I. Gurgan, N. Siddique, Y.-S. Li, S. Jang, G.A. Noh, S.H. Kim, Raman spectroscopy analysis of disordered and amorphous carbon materials: a review of empirical correlations, Carbon. N. Y. 238 (2025) 120214, https://doi.org/10.1016/j.carbon.2025.120214.
[36] S. Bettini, M. Ottolini, R. Pagano, S. Pal, A. Licciulli, L. Valli, G. Giancane, Coffee grounds-derived CNPs for efficient Cr(VI) water remediation, Nanomater. (Basel) 11 (2021) 1064, https://doi.org/10.3390/nano11051064.
[37] P. Zhang, J. Fan, Y. Wang, Y. Dang, S. Heumann, Y. Ding, Insights into the role of defects on the Raman spectroscopy of carbon nanotube and biomass-derived carbon, Carbon. N. Y. 222 (2024) 118998, https://doi.org/10.1016/j.carbon.2024.118998.
[38] W. Fawaz, J. Hasian, I. Alghoraibi, Synthesis and physicochemical characterization of carbon quantum dots produced from folic acid, Sci. Rep. 13 (2023), https://doi.org/10.1038/s41598-023-46084-1.
[39] G. Zhong, S. Xu, Q. Dong, X. Wang, L. Hu, Rapid, universal surface engineering of carbon materials via microwave-induced carbothermal shock, Adv. Funct. Mater. 31 (2021), https://doi.org/10.1002/adfm.202010968.
[40] Q. Huang, D. Qin, Y. Xia, Seeing is believing: what is on the surface of silver nanocrystals suspended in their original reaction solution, Chem. Sci. 15 (2024) 6321–6330, https://doi.org/10.1039/D4SC00730A.
[41] F.X. Liu, T.Z. Li, H.F. Zhang, Raman scattering from nanocrystalline Ag compacted under different pressures, Phys. Stat. Sol. 201 (2004) 776–781, https://doi.org/10.1002/pssa.200306755.
[42] E.S. Harsha Haridas, S. Bhattacharya, M.K.R. Varma, G.K. Chandra, Bioinspired 5-caffeoylquinic acid capped silver nanoparticles using Coffee arabica leaf extract for high-sensitive cysteine detection, Sci. Rep. 13 (2023) 8651, https://doi.org/10.1038/s41598-023-34944-9.
[43] N. Joshi, N. Jain, A. Pathak, J. Singh, R. Prasad, C.P. Upadhyaya, Biosynthesis of silver nanoparticles using Carissa carandas berries and its potential antibacterial activities, J. Sol-Gel. Sci. Technol. 86 (2018) 682–689, https://doi.org/10.1007/s10971-018-4666-2.
[44] X. Li, M. Gu, F. Zhang, Q. Min, L. Chen, Effects of raw materials on the structures of three dimensional graphene/amorphous carbon composites derived from biomass resources, Res. Chem. Intermed. 45 (2019) 1131–1145, https://doi.org/10.1007/s11164-018-3669-5.
[45] S.M. Mousavi, A.R. Mahjoub, R. Abazari, Green synthesis of ZnO hollow sphere nanostructures by a facile route at room temperature with efficient photocatalytic dye degradation properties, RSC. Adv. 5 (2015) 107378–107388, https://doi.org/10.1039/C5RA19507A.
[46] M.D. Hossain, Q. Zhang, T. Cheng, W.A. Goddard, Z. Luo, Graphitization of low-density amorphous carbon for electrocatalysis electrodes from ReaxFF reactive dynamics, Carbon. N. Y. 183 (2021) 940–947, https://doi.org/10.1016/j.carbon.2021.07.080.
[47] H. Daoudi, A. Bouafia, S.E. Laouini, S. Meneceur, M. Fellah, A. Iqbal, G.A. El-Hiti, B. Selmi, In vitro and in silico study of biosynthesized silver nanoparticles using Nigella sativa extract against SARS-CoV-2 and Candida albicans, J. Mol. Liq. 405 (2024) 125059, https://doi.org/10.1016/j.molliq.2024.125059.
[48] M.B. Gawande, S.N. Shelke, R. Zboril, R.S. Varma, Microwave-assisted chemistry: synthetic applications for rapid assembly of nanomaterials and organics, Acc. Chem. Res. 47 (2014) 1338–1348, https://doi.org/10.1021/ar400309b.
[49] Z. Zhang, S. Sheng, R. Wang, M. Sun, Tip-enhanced raman spectroscopy, Anal. Chem. 88 (2016) 9328–9346, https://doi.org/10.1021/acs.analchem.6b02093.
[50] C. Wang, H. Shi, M. Yang, Y. Yan, E. Liu, Z. Ji, J. Fan, Facile synthesis of novel carbon quantum dots from biomass waste for highly sensitive detection of iron ions, Mater. Res. Bull. 124 (2020) 110730, https://doi.org/10.1016/j.materresbull.2019.110730.
[51] P. Uznanski, J. Zakrzewska, F. Favier, S. Kazmierski, E. Bryszewska, Synthesis and characterization of silver nanoparticles from (bis)alkylamine silver carboxylate precursors, J. NanoPart Res. 19 (2017) 121, https://doi.org/10.1007/s11051-017-3827-5.
[52] O. Sambalova, K. Thorwarth, N.V. Heeb, D. Bleiner, Y. Zhang, A. Borgschulte, A. Kroll, Carboxylate functional groups mediate interaction with silver nanoparticles in biofilm matrix, ACS. Omega 3 (2018) 724–733, https://doi.org/10.1021/acsomega.7b00982.
[53] M. Reale, S. Chandra, G. Buscarino, A. Emanuele, M. Cannas, O. Ikkala, A. Sciortino, F. Messina, Photoinduced charge separation in functional carbon–silver nanohybrids, Phys. Chem. Chem. Phys. 24 (2022) 12974–12983, https://doi.org/10.1039/D2CP00668E.